Driving Force Distribution and Control for EV With Four In-Wheel Motors: A Case Study of Acceleration on Split-Friction Surfaces

Yafei Wang, *Member, IEEE*, Hiroshi Fujimoto, *Senior Member, IEEE*, and Shinji Hara, *Fellow, IEEE*

***Abstract*—Motion stabilization for electric vehicles with four in-wheel motors has been extensively studied in recent years. While most of the previous works have tended to focus on the development of optimization algorithms for driving force distribution, this paper considers a global–local control scheme: the global controller coordinates wheel and vehicle motions to generate reference driving forces and the local controller further controls the generated force commands. Specifically, two approaches with different global control concepts are proposed. The first approach considers the redesign of weighting factors for a conventional driving force optimization algorithm, and based on the first method, the second approach formulates the objective function and equality constraints in a two degree-of-freedom control framework. As an example, vehicle start off on an instantaneous split-friction road is employed to verify the proposed methods in both simulations and experiments.**

***Index Terms*—Driving force, electric vehicle (EV), in-wheel motor (IWM), motion control.**

Nomenclature

T	Time constant of driving force observers.
μ_i	Friction coefficient between the ith wheel and road.
λ_i	Slip ratio of the ith wheel.
ω_i	ith wheel's angular velocity.
ax	longitudinal acceleration rate.
df	Tread width.
r	Wheel radius.
k_i	Driving force distribution ratio of the ith wheel.
l	Lagrangian multiplier.
K_I	Integral gain for the inner wheel velocity control.
K_P	Proportional gain for the inner wheel velocity control.
$D_{s,i}$	Driving stiffness of the ith wheel.
$D'_{s,i}$	Slope of the $\mu_i - \lambda_i$ curve.
F_{all}	Total driving force.
F^*_{all}	Total driving force command.
F_{roll}	Rolling resistance.
F_i	Driving force of the ith wheel.
J_i	Rotational inertia of the ith wheel.
$J_{n,I}$	Nominal value of J_i.
N_i	Normal force of the ith wheel.
M	Vehicle mass.
T_i	Driving torque applied to the ith wheel.
$V_{\omega,I}$	Velocity of the ith wheel.
V_x	Vehicle velocity.
M^*_z	Desired yaw moment.

Manuscript received September 10, 2015; revised February 29, 2016 and May 23, 2016; accepted June 12, 2016. Date of publication September 27, 2016; date of current version March 8, 2017.

Y. Wang is with the School of Mechanical Engineering, Shanghai Jiao Tong University, Shanghai 200240, China (e-mail: wangyafei524@gmail.com).

H. Fujimoto is with the Department of Advanced Energy, Graduate School of Frontier Sciences, The University of Tokyo, Chiba 277-8561, Japan (e-mail: fujimoto@k.u-tokyo.ac.jp).

S. Hara is with the Department of Information Physics and Computing, Graduate School of Information Science and Technology, The University of Tokyo, Tokyo 113-8656, Japan (e-mail: Shinji_Hara@ipc.i.u-tokyo.ac.jp).

Color versions of one or more of the figures in this paper are available online at http://ieeexplore.ieee.org.

Digital Object Identifier 10.1109/TIE.2016.2613838

I. Introduction

AIMED at motion stabilization, driving force allocation and control for electric vehicles (EVs) with multiple driving motors have long been investigated [1]–[4], and most of the related studies consider the changes in the condition of one or more wheels, e.g., sudden change in road friction. Utilizing the advantages of motors, some studies focused on pure antislip control [5]–[7]. However, in addition to wheel slippage suppression, vehicle motion control is also necessary in some typical testing scenarios such as split-friction acceleration [8]. For traditional vehicles, the combination of active steering and differential braking was widely employed as control inputs [9], [10]. For an EV with four in-wheel motors (IWMs), the actuation flexibility of the wheels enables vehicle motion and wheel slip to be controlled together by adjusting the driving forces. For example, Sakai *et al.* demonstrated that direct yaw control (DYC) alone could not guarantee the stability of a 4 wheel-driven (4WD) EV on a slippery surface, and, hence, proposed an antiskid-based DYC [11]. As the vehicle was modeled as a half car, driving force distribution was not explicitly addressed. Driving force distribution is critical for vehicle motion stabilization and has been widely studied in recent years. In [12], a driver assistant system for a 4WD EV was studied by Tahami *et al*. who proposed a fuzzy logic algorithm to control both yaw motion and wheel slip, and simulations show good yaw rate tracking and accurate wheel slip control when braking on a split-friction surface. Another study conducted by Wang *et al.* considered the control of longitudinal speed and yaw rate on a low friction road, and formulated a cost function to address both wheel slip and vehicle motion [13]. One of the contributions of this literature was

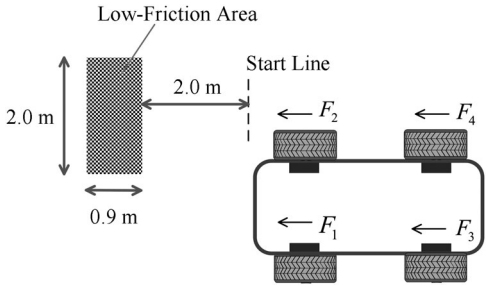

Fig. 1. Illustration of the research scenario.

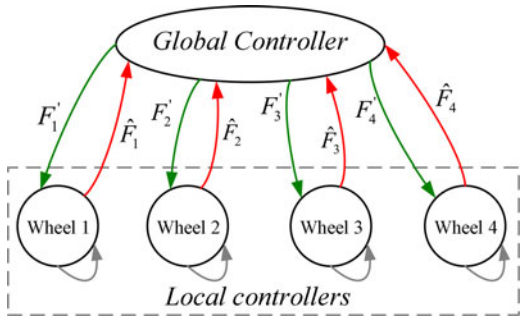

Fig. 2. Global–local control scheme for an EV with four IWMs.

the derivation of an analytical solution to the control allocation algorithm. In [14], an optimal torque distribution strategy for a 4WD EV was developed by considering multiple performance indices such as driving force and yaw moment, and was tested in slippery road conditions. Some other works considered energy efficiency in the design of objective function, e.g., Abe *et al*. designed an objective function to minimize tire dissipation energy [15], and Pennycott *et al*. considered maximizing the regenerative power produced during braking maneuvers [16]. These literatures have tended to focus on the development of driving force distribution methodologies, i.e., on how to generate feedforward control references for vehicle motion stability. However, as an IWM is attached to a tire, disturbances and complex tire dynamics inevitably influence the output force, especially on slippery roads. Therefore, local driving force controllers are indispensable [17], [18]. Considering this, motion control in split-/low-friction conditions was also performed in [19] and [20], in which a cost function similar to that proposed in [13] was constructed to distribute the driving force among the four wheels. Moreover, the driving forces were further controlled in the inner control loop. However, actual vehicle forces were not addressed in the optimization, and inevitably the control performances were adversely affected. That is, as the global distribution algorithm allocates driving forces, actual delivered forces should be addressed in the global optimization algorithm.

In this paper, a typical testing scenario, vehicle start off on an instantaneous split-friction road, is considered as an example to study driving force control. Such a condition is illustrated in Fig. 1. The uncontrolled driving wheel may experience slip due to the low friction, and the driving force commands can hardly be well achieved. Moreover, a sudden decrease of one driving force can generate undesired yaw motion. To accelerate the vehicle straight ahead without excessive tire slip, three factors are considered in the driving force control: 1) the wheel-road contacting conditions change rapidly when the vehicle enters or leaves the low-friction area, and locally controlling the wheel dynamics is desirable; 2) the control of wheel slip and vehicle motion both vary the torque applied to each wheel, and they should be coordinated to generate the reference driving forces. Moreover, actual driving forces need to be addressed in the generation of control efforts; 3) considering that an EV with four IWMs has a distributed structure, the control system can be formulated in a global–local way, where the local controllers suppress wheel slip and minimize the difference between the reference and actual driving forces, and global optimization provides the driving force commands. The remainder of this paper is organized as follows. In Section II, system modeling and the design of the local driving force controller are presented. In Section III, by considering vehicle acceleration on an instantaneous split-friction road, two proposed global controllers are explained together with a conventional controller. Next, Section IV presents simulation and experimental results. Finally, conclusions and future works are provided in Section V.

II. System Modeling for Local Driving Force Control

As illustrated in Fig. 2, an EV with four IWMs can be considered as a global control system with four local agents, in which the global and the four wheel controllers exchange reference and actual driving forces. In this section, basic wheel and vehicle dynamics are introduced for the design of the local driving force controllers.

A. Vehicle and Wheel Dynamics

The longitudinal motion of a 4WD vehicle can be described as (1). As this term is small and usually not controllable, it is neglected in the controller design

$$M \cdot \dot{V}_x = F_{\text{all}} - F_{\text{roll}} = \sum_{i=1}^{4} F_i - F_{\text{roll}} \tag{1}$$

where

$$F_i = k_i \cdot F_{\text{all}}.$$

For a single wheel, the governing dynamics equation and slip ratio can be given as (2) and (3), respectively. As the wheel radiuses of high-speed vehicles are often the same, r is used instead of r_i in this paper

$$J_i \cdot \dot{\omega}_i = T_i - F_i \cdot r \tag{2}$$

$$\lambda_i = \frac{V_{\omega,i} - V_x}{\max(V_{\omega,i}, V_x)} \tag{3}$$

where $V_{\omega,i} = \omega_i \cdot r$, and $V_{\omega,i}$ is greater than V_x when accelerating and is less than V_x when decelerating. In Fig. 3, a typical curve of friction coefficient versus slip ratio is illustrated, and F_i can be represented as

$$F_i = \mu_i(\lambda_i) \cdot N_i. \tag{4}$$

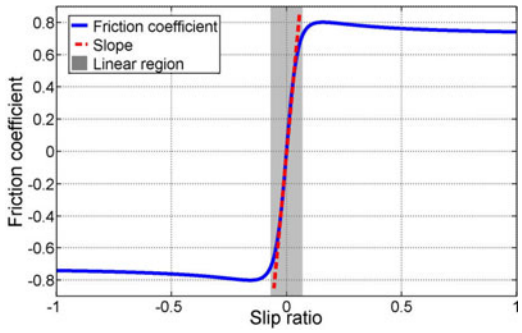

Fig. 3. Typical curve of friction coefficient versus slip ratio.

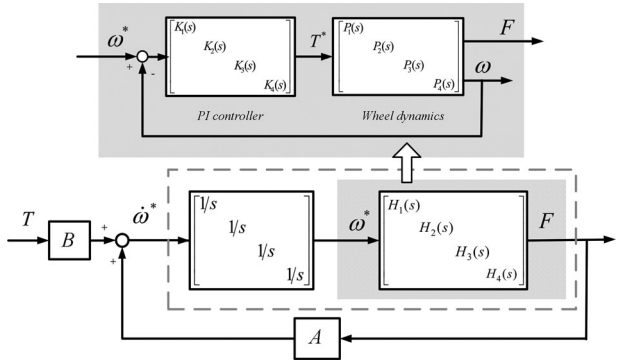

Fig. 4. Block diagram of the local driving force controller.

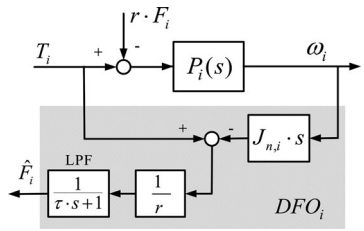

Fig. 5. Principle of the DFO.

The shaded area of Fig. 3 represents the linear region of the curve, and the slope is defined as $D'_{s,i}$. Then, F_i can be further represented as (5) by introducing driving stiffness $D_{s,i}$ [19]

$$F_i = D_{s,i} \cdot \lambda_i, \text{ where } D_{s,i} \doteq D'_{s,i} \cdot N_i. \tag{5}$$

B. Driving Force Control With Driving Force Observer (DFO)

As previously explained, most of the existing works on driving force distribution and control treated the problems from the perspective of optimization. However, when a vehicle traverses on a low-/split-friction surface where the tire slip may differ from wheel to wheel, desired wheel and vehicle motions are not achievable without some kinds of driving force control. In this section, a driving force control method based on DFO is introduced.

From (2), the angular acceleration of the *i*th wheel is obtained as

$$\dot{\omega}_i = \frac{1}{J_i}(T_i - F_i \cdot r_i) \tag{6}$$

and a state-space formulation can then be constructed for the four wheels as

$$\dot{\omega} = A \cdot F + B \cdot T \tag{7}$$

where

$$\omega = \left[\omega_1,\ \omega_2,\ \omega_3,\ \omega_4\right]^T,\ F = \left[F_1,\ F_2,\ F_3,\ F_4\right]^T$$
$$T = \left[T_1,\ T_2,\ T_3,\ T_4\right]^T$$
$$A = \text{diag}\left(\frac{-r}{J_1}, \frac{-r}{J_2}, \frac{-r}{J_3}, \frac{-r}{J_4}\right)$$
$$B = \text{diag}\left(\frac{1}{J_1}, \frac{1}{J_2}, \frac{1}{J_3}, \frac{1}{J_4}\right).$$

Now, the overall control system can be formulated as Fig. 4.

Another formulation of the driving force controller can be found in [19]. In addition, (8) can be obtained from (2)

$$\sum_{i=1}^{4}(J_i \cdot \dot{\omega}_i) = \sum_{i=1}^{4} T_i - r \cdot \sum_{i=1}^{4} F_i. \tag{8}$$

Next, by substituting (1) into (8), the relationship between the input torque and the output wheel angular velocity can be obtained as

$$\sum_{i=1}^{4} T_i = \sum_{i=1}^{4}(J_i \cdot \dot{\omega}_i) + M \cdot r^2 \cdot \dot{\omega}_i. \tag{9}$$

For the *i*th wheel, the dynamics can be nominalized as (10) based on (9):

$$P_i(s) = \frac{\omega_i}{T_i} = \frac{1}{\left(\frac{M \cdot r^2}{4} + J_i\right) \cdot s} := \frac{1}{\Delta_{G,i} \cdot s}. \tag{10}$$

Assuming the wheel velocity is controlled by a PI controller, the inner loop transfer function of Fig. 4 is derived as

$$H_i(s) = \frac{K_P \cdot s + K_I}{\Delta_{G,i} \cdot s^2 + K_P \cdot s + K_I}. \tag{11}$$

To obtain driving forces for the feedback loops, observers are needed. In general, there are two types of DFO. One type is a closed-loop observer such as the observer designed in [21], but such a method is too complicated to be used online. In this study, a disturbance observer is employed, and its principle is illustrated in Fig. 5. The basic idea is to treat $r \cdot F_i$ as disturbance, and as T_i is available and ω_i can be measured by a wheel encoder, $r \cdot \hat{F}_i$ can be calculated using (2). Note that the estimate from DFO not only contains driving force, but also includes real disturbances. In practice, to suppress sensor noise, ω_i can be processed by a low-pass filter (LPF) with a cut off frequency of 30 Hz. In the observer shown in Fig. 5, the LPF is used to guarantee causality, and τ is the time constant. The driving force estimate is represented as

$$\hat{F}_i = \frac{T_i - J_{n,i} \cdot \omega_i \cdot s}{r} \cdot \frac{1}{\tau \cdot s + 1}. \tag{12}$$

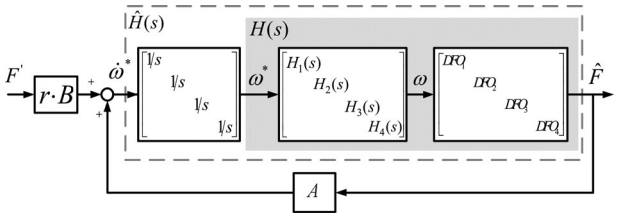

Fig. 6. Local driving force controller with DFOs.

Thus, Fig. 4 can be further represented as Fig. 6 by including the DFOs, where $\hat{H}_i(s)$ is defined as $H_i(s)/s$. F' is a vector of the four driving force commands. Note that the control scheme introduced above serves as an inner loop in the whole control system.

III. Global Control System: A Case Study of Acceleration on Instantaneous Split Friction Roads

As previously introduced, a typical scenario to test motion control performance is start off on an instantaneous split-friction road. When a driving wheel reaches a low-friction surface, the slip ratio increases and the driving force is saturated and reduced. This is especially undesired in the case of split-friction conditions, as a yaw motion is generated if the left and right driving forces are different. Therefore, the four driving forces need to be adjusted allowing the vehicle to accelerate straight ahead. Moreover, the slip ratio of each wheel needs to be suppressed.

A. Brief Review of the Conventional Method

Conventional method: In [19], to minimize the slip ratios, a cost function J_1 is defined in (13) as the sum of the squares of λ_i. Specifically, as $D_{s,i}$ is difficult to measure, it is estimated as $\hat{D}_{s,i}$ using a recursive least squares method

$$\begin{aligned} J_1 &= \lambda_1^2 + \lambda_2^2 + \lambda_3^2 + \lambda_4^2 \\ &= \frac{F_1^2}{\hat{D}_{s,1}^2} + \frac{F_2^2}{\hat{D}_{s,2}^2} + \frac{F_3^2}{\hat{D}_{s,3}^2} + \frac{F_4^2}{\hat{D}_{s,4}^2}. \end{aligned} \tag{13}$$

To avoid undesired acceleration and yaw motion, the total driving force and yaw moment are considered as equality constraints. That is, having the two constraints satisfied while minimizing the slip ratios is desirable. The objective function with the two constraints is given as (14), where M_z^* is zero in the case of straight driving. To represent commands, F' is used instead of F as

$$\min \quad f = \frac{1}{2} \cdot (F')^{\mathrm{T}} \cdot W \cdot F', \text{ s.t. } B \cdot F' = b$$

where

$$\begin{aligned} F' &= \left[F_1', F_2', F_3', F_4'\right]^{\mathrm{T}} \\ W &= \operatorname{diag}\left(1/\hat{D}_{s,1}^2, 1/\hat{D}_{s,2}^2, 1/\hat{D}_{s,3}^2, 1/\hat{D}_{s,4}^2\right) \\ B &= \begin{bmatrix} 1 & 1 & 1 & 1 \\ \frac{-d_f}{2} & \frac{d_f}{2} & \frac{-d_f}{2} & \frac{d_f}{2} \end{bmatrix}, \; b = \begin{bmatrix} F_{\mathrm{all}}^* \\ M_z^* \end{bmatrix}. \end{aligned} \tag{14}$$

To solve the above problem, first define a Lagrangian function as

$$L = \frac{1}{2} \cdot (F')^{\mathrm{T}} \cdot W \cdot F' + l \cdot (B \cdot F' - b) \tag{15}$$

and then, take the partial derivative of L with respect to F' and l, and set them to zero

$$\begin{aligned} \nabla_{F'} L &= (F')^{\mathrm{T}} \cdot W + l \cdot B = 0 \\ \nabla_l L &= B \cdot F' - b = 0. \end{aligned} \tag{16}$$

Finally, from (16), the Lagrangian multiplier and the desired driving forces can be obtained as

$$\begin{aligned} l &= -\left(B \cdot W \cdot B^{\mathrm{T}}\right)^{-1} \cdot b \\ F' &= W \cdot B^T \cdot \left(B \cdot W \cdot B^{\mathrm{T}}\right)^{-1} \cdot b. \end{aligned} \tag{17}$$

B. Proposed Methods

Proposed method 1: As can be seen in (13), the weighting factor for each λ_i^2 is set as 1. However, as the slippery conditions are different for each wheel, they should be weighted based on some rules [22]. Considering that the road-contacting conditions of the four wheels may not be the same, a rule is set to equalize the four slip ratios such that $\lambda_1 = \lambda_2 = \lambda_3 = \lambda_4 \doteq \lambda_i$. By considering (5) of the four wheels, (18) can be obtained as

$$F_{\mathrm{all}} = (D_{s,1} + D_{s,2} + D_{s,3} + D_{s,4}) \cdot \lambda_i. \tag{18}$$

Next, combining (1), (5), and (18) yields (19), where $\hat{D}_{s,i}$ is used instead of $D_{s,i}$

$$k_i = \frac{\hat{D}_{s,i}}{\hat{D}_{s,1} + \hat{D}_{s,2} + \hat{D}_{s,3} + \hat{D}_{s,4}} \doteq k_{e,i}. \tag{19}$$

Next, by adding weighting factors ξ_1, ξ_2, and ξ_3 into (14), the objective function (20) can be formulated as

$$\begin{aligned} J_2 &= \zeta_1 \cdot \lambda_1^2 + \zeta_2 \cdot \lambda_2^2 + \zeta_3 \cdot \lambda_3^2 + \lambda_4^2 \\ &= \left[\frac{\zeta_1 \cdot k_1^2}{\hat{D}_{s,1}^2} + \frac{\zeta_2 \cdot k_2^2}{\hat{D}_{s,2}^2} + \frac{\zeta_3 \cdot k_3^2}{\hat{D}_{s,3}^2} \right. \\ &\quad \left. + \frac{\zeta_4 \cdot (1 - k_1 - k_2 - k_3)^2}{\hat{D}_{s,4}^2}\right] \cdot F_{\mathrm{all}}^2. \end{aligned} \tag{20}$$

To minimize J_2, k_i should satisfy $\partial J_2 / \partial k_i = 0$, thus yielding

$$\begin{aligned} k_1 &= \frac{\zeta_2 \cdot \zeta_3 \cdot \hat{D}_{s,1}}{\Delta} \doteq k_{w,1}, \; k_2 = \frac{\zeta_1 \cdot \zeta_3 \cdot \hat{D}_{s,2}}{\Delta} \doteq k_{w,2} \\ k_3 &= \frac{\zeta_1 \cdot \zeta_2 \cdot \hat{D}_{s,3}}{\Delta} \doteq k_{w,3}, \; k_4 = \frac{\zeta_1 \cdot \zeta_2 \cdot \zeta_3 \cdot \hat{D}_{s,4}}{\Delta} \doteq k_{w,4} \end{aligned} \tag{21}$$

where

$$\begin{aligned} \Delta = \zeta_2 \cdot \zeta_3 \cdot \hat{D}_{s,1} + \zeta_1 \cdot \zeta_3 \cdot \hat{D}_{s,2} + \zeta_1 \cdot \zeta_2 \cdot \hat{D}_{s,3} \\ + \zeta_1 \cdot \zeta_2 \cdot \zeta_3 \cdot \hat{D}_{s,4}. \end{aligned}$$

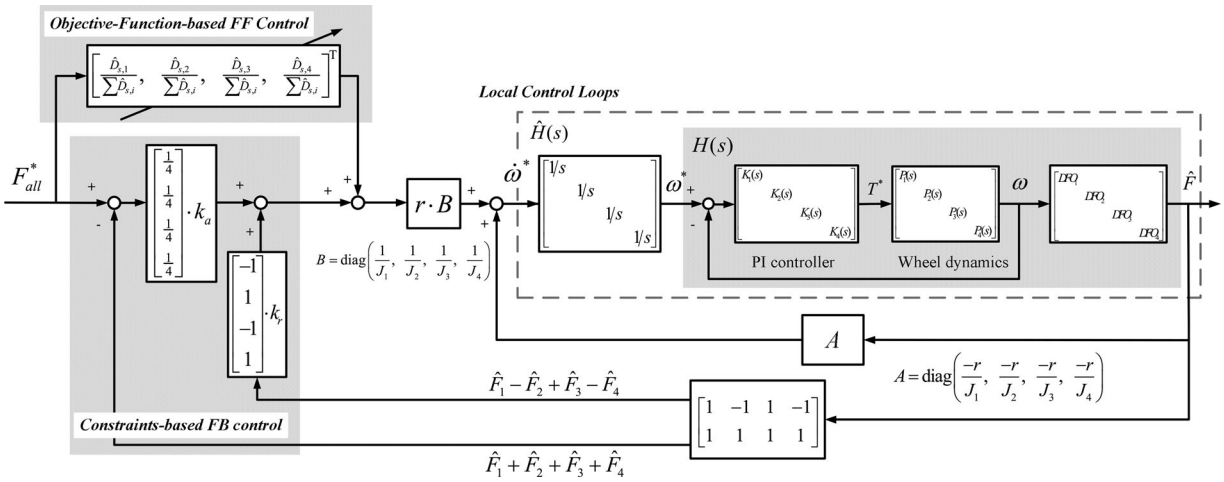

Fig. 7. Proposed global–local control scheme.

By equalizing $k_{e,i}$ and $k_{w,i}$, the weighting factors can be obtained as (22). That is, by designing the weighting factors as (22), the four slip ratios can be equalized

$$\zeta_1 = \frac{\hat{D}_{s,1}}{\hat{D}_{s,4}},\ \zeta_2 = \frac{\hat{D}_{s,2}}{\hat{D}_{s,4}},\ \zeta_3 = \frac{\hat{D}_{s,3}}{\hat{D}_{s,4}}. \tag{22}$$

Finally, the weighted cost function J_2 is obtained as (23) based on (14) and (22)

$$J_2 = \left(\frac{F_1^2}{\hat{D}_{s,1}} + \frac{F_2^2}{\hat{D}_{s,2}} + \frac{F_3^2}{\hat{D}_{s,3}} + \frac{F_4^2}{\hat{D}_{s,4}}\right) \cdot \frac{1}{\hat{D}_{s,4}}. \tag{23}$$

The constraints of this method are the same as those of the conventional method, and the force references can also be calculated using the conventional optimization approach given in (15)–(17).

Proposed method 2 (Optimization-based 2DOF control approach). As explained in Section I, disturbances and complex tire dynamics influence the output forces of the wheels. Therefore, the mismatches between reference and actual driving forces inevitably influence the longitudinal and yaw motions. Unfortunately, this was not considered in conventional optimization algorithms. To represent actual vehicle behavior in the control algorithm, signals such as yaw rate can be employed. In this study, instead of using additional sensors, estimated driving forces are utilized to construct the feedback loops, and the optimization of an objective function with equality constraints is interpreted in a 2DOF scheme.

First, reuse the weighted objective function (23) and formulate it as (24) by using the definition of (1):

$$J_2 = \left[\frac{k_1^2}{\hat{D}_{s,1}} + \frac{k_2^2}{\hat{D}_{s,2}} + \frac{k_3^2}{\hat{D}_{s,3}} + \frac{(1-k_1-k_2-k_3)^2}{\hat{D}_{s,4}}\right] \cdot \frac{(F_{\text{all}}^*)^2}{\hat{D}_{s,4}}. \tag{24}$$

Then, by solving the partial differential equation $\partial J_2 / \partial k|_{k=k_i} = 0$, optimal k_i without considering the constraints can be obtained as (25). This serves as a part of the feedforward term in the global controller

$$k_i = \frac{\hat{D}_{s,i}}{\hat{D}_{s,1} + \hat{D}_{s,2} + \hat{D}_{s,3} + \hat{D}_{s,4}}. \tag{25}$$

As the driving force terms in the equality constraints of (14) can be given by DFOs, (26) is defined by replacing F' with $\hat{F}$ as

$$F_{\text{all}}^* - \sum_{i=1}^{4} \hat{F}_i \doteq e_a,\ \ \hat{F}_1 - \hat{F}_2 + \hat{F}_3 - \hat{F}_4 \doteq e_r. \tag{26}$$

Therefore, the two constraints can be interpreted as two feedback loops by using the driving force estimates: one loop to minimize the difference between the delivered total driving force and the command, and another loop is to equalize the actual left and right driving forces. The overall control structure is illustrated in Fig. 7, where k_a and k_r are the gains that need to be tuned. Similar to the concept of weighting factor in an

TABLE I
SPECIFICATIONS OF THE EXPERIMENTAL SETUP

Vehicle Parameters	
Vehicle mass	850 kg
Height of center of gravity (CoG)	0.51 m
Distance from CoG to front axle	1.013 m
Distance from CoG to rear axle	0.702 m
Spin inertial of the ith wheel	1.24 kg·m^2 ($i = 1, 2$)/ 1.26 kg·m^2 ($i = 3, 4$)
Wheel radius	0.301 m
Tread width	1.3 m
Yaw inertial	617 kg·m^2
Vehicle Structure	
Suspension	Double wishbone
Controller	AutoBox DS1103
IWM	
Type	Direct drive outer rotor
Maximum Torque	500 N·m
Maximum Power	20 kW

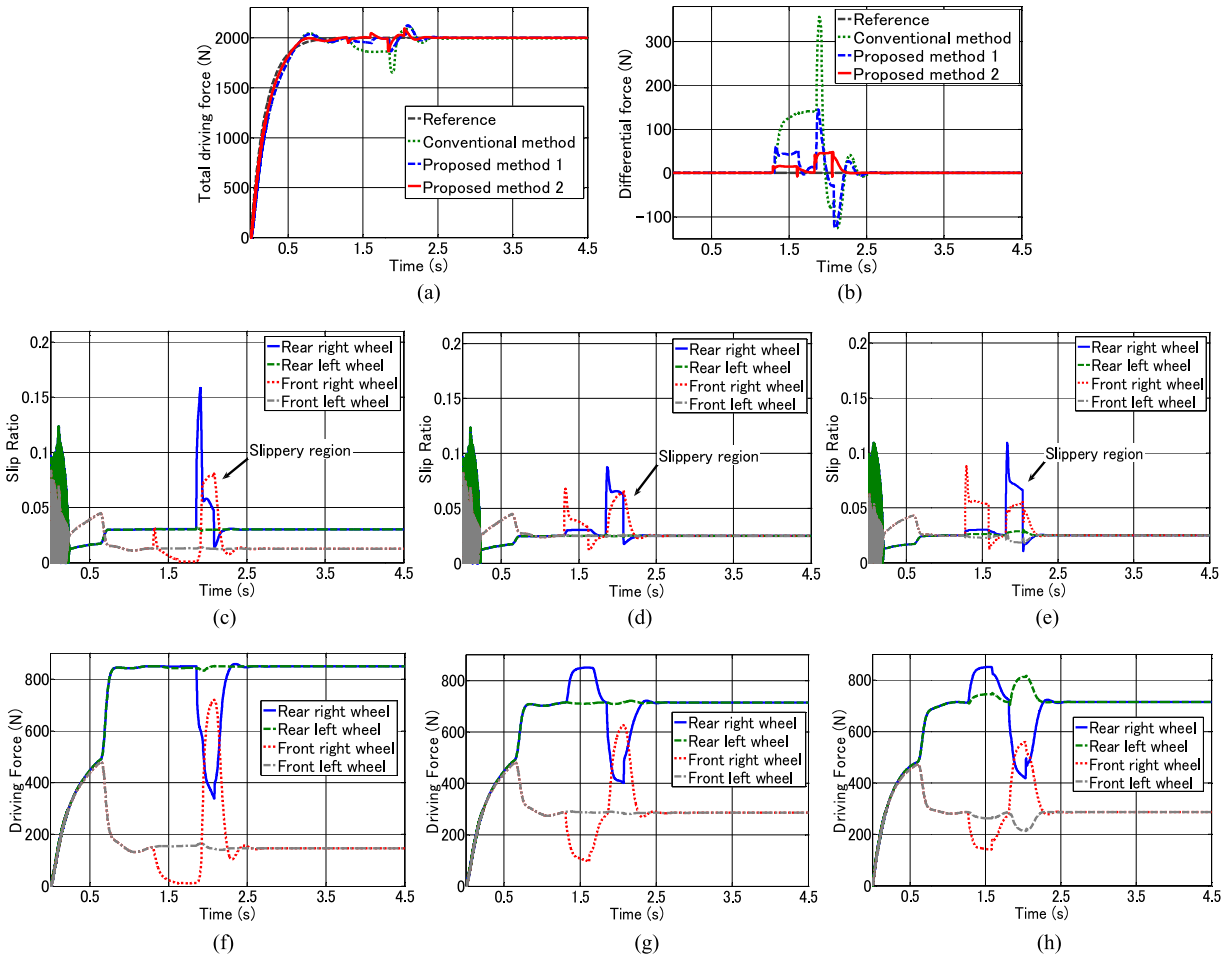

Fig. 8. Comparison of the three methods (simulation results): (a) Total driving force; (b) differential driving force; (c) slip ratio (conventional method); (d) slip ratio (proposed method 1); (e) slip ratio (proposed method 2); (f) individual force (conventional method); (g) individual force (proposed method 1); and (h) individual force (proposed method 2).

optimization algorithm, the two gains can be tuned by considering that: 1) if the total driving force needs to be well satisfied, k_a has to be increased, and 2) if it is desirable to reduce yaw motion, k_r needs to be increased.

IV. Simulations and Experiments

A. Simulations

The simulation scenario is shown in Fig. 1. The vehicle is assumed to accelerate in front of an instantaneous split-friction road and the friction coefficients for the high- and low-friction surfaces are 0.8 and 0.2, respectively. Clearly, the two left wheels are always on the high-friction road, and the two right wheels change from the high-friction road to a low-friction surface, and then change back to the high-friction road. In the simulation, to better represent actual vehicle dynamics, vehicle plant is considered as a 2DOF vehicle model with the Magic Formula-based tire model. Based on our experimental EV, the main vehicle parameters used in the simulations are provided in Table I. During split-friction testing, the total driving force command increases from 0 to 2000 N, and the yaw moment/differential force reference is zero.

The two proposed control methods are compared with the conventional method in terms of control performances. For fair comparison, the local controllers are set to be identical with a *P*-gain of 49.6 and an *I*-gain of 496. k_a and k_r of the proposed method 2 are set to 1 and 4, respectively. The simulation results are provided in Fig. 8, and the slippery region is from approximately 1.3 to 2.1 s. Fig. 8(a) and (b) shows the reference following performances of the three methods, i.e., whether the two constraints in (15) are satisfied. The elements of the objective function in the conventional method are equally weighted, indicating that the slip ratios cannot be evenly minimized. Therefore, the total and differential driving forces vibrate in the slippery region. Because of the weighting factors, the vibration amplitude in the proposed method 1 is smaller than that in the conventional method. In the case of proposed method 2, as the actual driving forces are included in the control scheme, the reference tracking performances are the best among the three methods. Fig. 8(c)–(e) demonstrates the performances of the slip ratio control, i.e., indicate to which level the three objective functions are minimized. Clearly, all the three methods can suppress excessive wheel slip to less than 0.2. As the objective functions of the two

proposed methods are weighted, the slip ratios can be further minimized. Note that while the objective function has to be minimized, the constraints have to be satisfied at the same time, i.e., a tradeoff exits. Therefore, the slip ratios in the proposed method 2 are slightly greater than those in the proposed method 1. Nevertheless, both the methods can suppress wheel slippage to a reasonable level. The four distributed driving forces of the three methods are shown in Fig. 8(f)–(h), which demonstrate why the proposed approaches provide better reference tracking performance. At approximately 1.3 s, the front right wheel reaches the low-friction area, and the driving force, therefore, decreases significantly. In the conventional method, the other three forces remain unchanged and proposed method 1 increases the rear right driving force to stabilize the vehicle. By addressing actual output forces, the proposed method 2 adjusts the two left forces in addition to the rear right wheel. From approximately 1.9 s, the front right wheel leaves the low friction surface and the rear right wheel reaches that area; therefore, the rear right force decreases and the front right force increases. Again, the proposed approach adjusts the left two forces to guarantee the constraints to be well satisfied. Note that the driving force distributions and the slip ratios of the two proposed methods are similar as they share the same objective function, but the proposed method 2 can further modify the four forces by the actual driving force feedback.

B. Experiments

In the experiments, an original experimental EV with four permanent magnet-type IWMs [23] was utilized. The vehicle is equipped with an onboard dSPACE AutoBox-DS1103 for real-time data acquisition and control, and the algorithms in this study were implemented using a model-based design approach. The specification of this vehicle is given in Table I. Owing to manufacturing differences, the wheel inertias of the front and rear wheels are not the same, but the proposed methods are also applicable to EVs with four identical IWMs. The experimental scenario is shown in Fig. 9. As can be seen, the vehicle starts from a high-friction road and then enters a split-friction surface. The low-friction surface is a polymer plastic sheet with water on it, and the friction coefficient is approximately 0.2. As in the simulations, the friction coefficients of the two left wheels are always high, and the friction coefficients of the two right wheels change from high to low, and then change back to high again. The total driving force command increases from 0 to 2000 N, and the yaw moment/differential force reference is zero.

Again, for fair comparison, the local controllers in the experiments were set to be identical, and the gains were chosen to be the same as the gains in the simulations. The experimental results are provided in Fig. 10, and the slippery region is from approximately 1.3 to 2.5 s. Fig. 10(a) and (b) shows the comparison of the total driving force and differential force, respectively; the green lines represent the results using the conventional method. Obviously, the reference tracking performance is not satisfactory, and the reason can be found in Fig. 10(f).

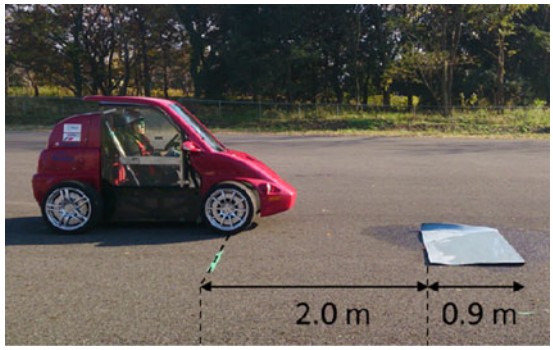

Fig. 9. Experimental setup.

In the conventional method, the driving forces of the two front wheels are almost 0 N on the high-friction road. Therefore, the total driving force was reduced and the differential force could not be further adjusted. In other words, the two constraints in (15) could not be well satisfied. Fig. 10(c) shows the control performance in terms of the slip ratio. Although the slip ratio was controlled to be less than 0.2, the rear right slip ratio could not be further suppressed, and it is different from the other three on the low-friction surface. This is because the four slip ratio squares of the objective function are equally weighted, and when the rear right wheel is on the low-friction surface, its slip ratio cannot be further minimized as the other three slip ratios are low. The blue lines in Fig. 10(a) and (b) show reference tracking performances of the proposed method 1, and the vibration amplitudes of the total driving force and differential force are smaller than that obtained in the conventional method. The reason can be determined by analyzing the results in Fig. 10(d) and (g). As shown in Fig. 10(d), the four slip ratios are equalized because of the weighting factors; as shown in Fig. 10(g), the start values of the four forces are in the same level, providing the possibility to adjust the four forces to a certain extent. This is not possible in the conventional method as the two left forces are almost zero. The proposed method 2 shares the same objective function with the proposed method 1, and their slip ratio results are, therefore, very similar, and can be observed in Fig. 10(d) and (e). However, they are different in the handling of the two constraints, i.e., the proposed method 2 can further modify the four forces by the feedback of actual driving forces, which is especially important on a low-friction road. Therefore, the red lines in Fig. 10(a) and (b) that represent the proposed method 2 track the reference as the best among the three methods. In summary, Fig. 10(a) and (b) demonstrates the reference tracking performances of the three methods and can show whether the constraints are satisfied. Clearly, the proposed method 2 is better than the other two methods because the actual output forces are employed. Fig. 10(c)–(e) shows the results of slip ratio control performances, which are the indices that show whether the three objective functions are achieved. Clearly, all the three methods can suppress excessive wheel slip, but the rear right slip ratio with the conventional method is not very satisfactory. As the objective functions of the two proposed methods are the same, their slip ratios are similar.

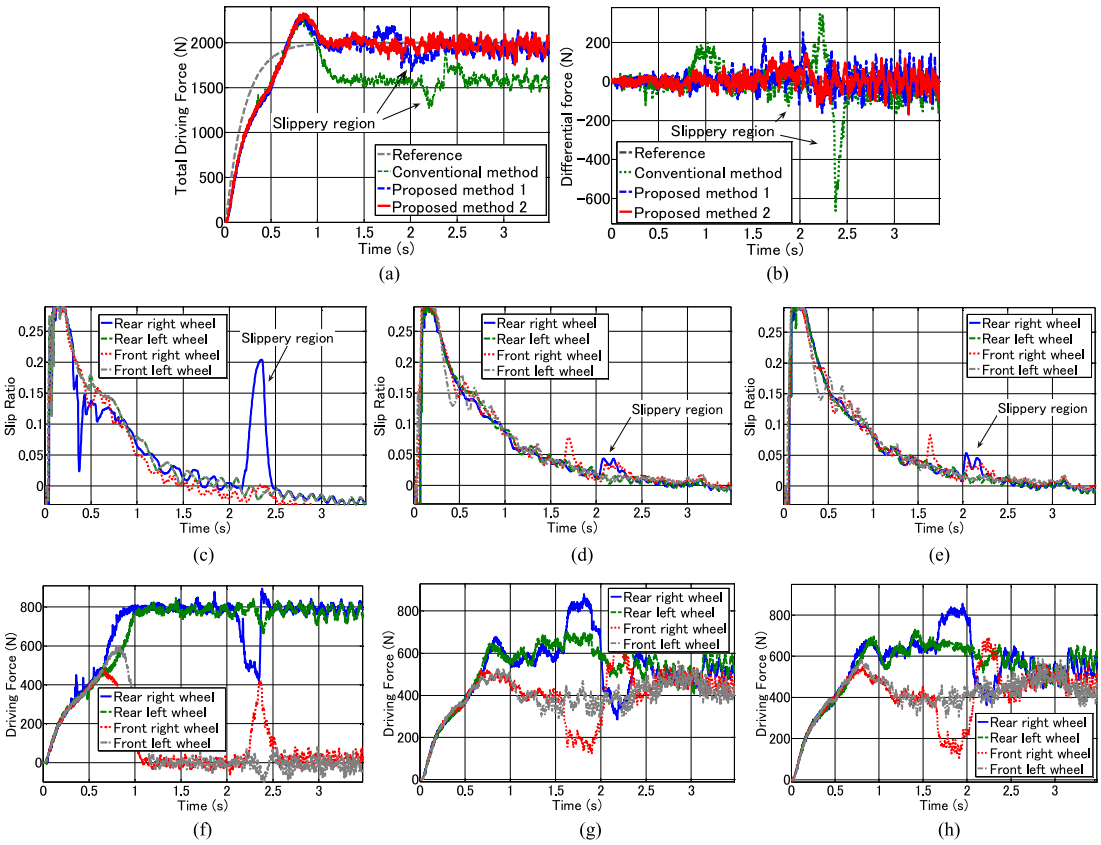

Fig. 10. Comparison of the three methods (experimental results): (a) Total driving force; (b) differential driving force; (c) slip ratio (conventional method); (d) slip ratio (proposed method 1); (e) slip ratio (proposed method 2); (f) individual force (conventional method); (g) individual force (proposed method 1); and (h) individual force (proposed method 2).

V. Conclusion and Future Work

This paper considered driving force distribution and control of an EV with four IWMs. As an example, vehicle start off on an instantaneous split-friction surface was investigated, with the objective to keep the total driving force following the reference and to keep the vehicle running straight without excessive wheel slip. In this study, we studied two global–local control-based methods by introducing local driving force control. Aimed at equalizing the four slip ratios, the first method considered the redesign of weighting factors for a conventional driving force optimization algorithm. Based on the first method, the second proposed method interpreted the objective function and equality constraints in a 2DOF control scheme. The feedforward and feedback controllers were designed based on the objective function and the constraints, respectively. Moreover, the two proposed control schemes were compared with a conventional scheme in both simulations and experiments. As pointed out in [24], many open issues related to driving force control of 4WD vehicles still exist, and these issues can be considered in the global–local control framework in future works. In addition, greater control freedom can be achieved by introducing a steer-by-wire technology [25], [26], and the coordination of driving and steering has to be considered for achieving better control performances.

References

[1] Y. Hori, "Future vehicle driven by electricity and control—Research on 4 wheel motored "UOT March II,"" *IEEE Trans. Ind. Electron.*, vol. 51, no. 5, pp. 954–962, Oct. 2004.

[2] K. Nam, S. Oh, H. Fujimoto, and Y. Hori, "Estimation of sideslip and roll angles of electric vehicles using lateral tire force sensors through RLS and Kalman filter approaches," *IEEE Trans. Ind. Electron.*, vol. 60, no. 3, pp. 988–1000, Mar. 2013.

[3] N. Mutoh, "Driving and braking torque distribution methods for front- and rear-wheel-independent drive-type electric vehicles on roads with low friction coefficient," *IEEE Trans. Ind. Electron.*, vol. 59, no. 10, pp. 3919–3933, Oct. 2012.

[4] S. Kuntanapreeda, "Traction control of electric vehicles using sliding-mode controller with tractive force observer," *Int. J. Veh. Technol.*, vol. 2014, 2014, Art. no. 829097.

[5] A. Dadashnialehi, A. Bab-Hadiashar, Z. Cao, and A. Kapoor, "Intelligent sensorless antilock braking system for brushless in-wheel electric vehicles," *IEEE Trans. Ind. Electron.*, vol. 62, no. 3, pp. 1629–1638, Mar. 2015.

[6] D. Yin, S. Oh, and Y. Hori, "A novel traction control for EV based on maximum transmissible torque estimation," *IEEE Trans. Ind. Electron.*, vol. 56, no. 6, pp. 2086–2094, Jun. 2009.

[7] R. de Castro, R. Araujo, and D. Freitas, "Wheel slip control of EVs based on sliding mode technique with conditional integrators," *IEEE Trans. Ind. Electron.*, vol. 60, no. 8, pp. 3256–3271, Aug. 2013.

[8] A. E. Jackson, "Intelligent mobility control of a hybrid electric off-road vehicle with individual wheel control" Ph.D. dissertation, Sch. Mech. Eng., Univ. Leeds, Leeds, U.K., 2003.

[9] J. Tjonnas and T. Johansen, "Stabilization of automotive vehicles using active steering and adaptive brake control allocation," *IEEE Trans. Control Syst. Technol.*, vol. 18, no. 3, pp. 545–558, May 2010.

[10] S. Di Cairano, H. E. Tseng, D. Bernardini, and A. Bemporad, "Vehicle yaw stability control by coordinated active front steering and differential braking in the tire sideslip angles domain," *IEEE Trans. Control Syst. Technol.*, vol. 21, no. 4, pp. 1236–1248, Jul. 2013.
[11] S. Sakai, H. Sado, and Y. Hori, "Motion control in an electric vehicle with four independently driven in-wheel motors," *IEEE/ASME Trans. Mechatronics*, vol. 4, no. 1, pp. 9–16, Mar. 1999.
[12] F. Tahami, R. Kazemi, and S. Farhanghi, "A novel driver assist stability system for all-wheel-drive electric vehicles," *IEEE Trans. Veh. Technol.*, vol. 52, no. 3, pp. 683–692, May 2003.
[13] R. Wang, H. R. Karimi, N. Chen, G. Yin, and J. Wang, "Motion control of four-wheel independently actuated electric ground vehicles considering tire force saturations," *Math. Probl. Eng.*, vol. 2013, 2013, Art. no. 819302.
[14] B. Li, A. Goodarzi, A. Khajepour, S. Chen, and B. Litkouhi, "An optimal torque distribution control strategy for four-independent wheel drive electric vehicles." *Veh. Syst. Dyn.*, vol. 53, no. 8, pp. 1172–1189, 2015.
[15] Y. Suzuki, Y. Kano, and M. Abe, "A study on tyre force distribution controls for full drive-by-wire electric vehicle," *Veh. Syst. Dyn.*, vol. 52, Suppl. 1, pp. 235–250, 2014.
[16] A. Pennycott, L. De Novellis, P. Gruber, and A. Sorniotti, "Optimal braking force allocation for a four wheel drive fully electric vehicle," *J. Syst. Control Eng.*, vol. 228, no. 8, pp. 621–628, Sep. 2014.
[17] B. C. Chen and C. C. Kuo, "Electronic stability control for electric vehicle with four in-wheel motors," *Int. J. Autom. Technol.*, vol. 15, no. 4, pp. 573–580, Jun. 2014.
[18] M. Gerard and M. Verhaegen, "Global and local chassis control based on load sensing," in *Proc. Amer. Control Conf.*, Jun. 2009, pp. 677–682.
[19] K. Maeda, H. Fujimoto, and Y. Hori, "Four-wheel driving-force distribution method for instantaneous or split slippery roads for electric vehicle," *Automatika*, vol. 54, no. 1, pp. 103–113, 2013.
[20] H. Fujimoto, J. Amada, and K. Maeda, "Review of traction and braking control for electric vehicle," in *Proc. Veh. Power Propulsion Conf.*, Oct. 2012, pp. 1292–1299.
[21] T. Hsiao, "Robust wheel torque control for traction/braking force tracking under combined longitudinal and lateral motion," *IEEE Trans. Intell. Transp. Syst.*, vol. 16, no. 3, pp. 1335–1347, Jun. 2015.
[22] S. Yim, "Fault-tolerant yaw moment control with steer and brake-by-wire devices," *Int. J. Autom. Technol.*, vol. 15, no. 3, pp. 463–468, Apr. 2014.
[23] H. Fujimoto and S. Harada, "Model-based range extension control system for electric vehicles with front and rear driving–braking force distributions," *IEEE Trans. Ind. Electron.*, vol. 62, no. 5, pp. 3245–3254, May 2015.
[24] V. Ivanov, D. Savitski, and B. Shyrokau, "A survey of traction control and antilock braking systems of full electric vehicles with individually controlled electric motors," *IEEE Trans. Veh. Technol.*, vol. 64, no. 9, pp. 3878–3896, Sep. 2015.
[25] H. Wang, H. Kong, Z. Man, D. M. Tuan, Z. Cao, and W. Shen, "Sliding mode control for steer-by-wire systems with AC motors in road vehicles," *IEEE Trans. Ind. Electron.*, vol. 61, no. 3, pp. 1596–1611, Mar. 2014.
[26] Z. Sun, J. Zheng, Z. Man, and H. Wang, "Robust control of a vehicle steer-by-wire system using adaptive sliding mode," *IEEE Trans. Ind. Electron.*, vol. 63, no. 4, pp. 2251–2262, Apr. 2016.

Yafei Wang (S'12–M'14) received the B.S. degree in internal combustion engines from Jilin University, Changchun, China, in 2005, the M.S. degree in vehicle engineering from Shanghai Jiao Tong University, Shanghai, China, in 2008, and the Ph.D. degree in electrical engineering from The University of Tokyo, Tokyo, Japan, in 2013.

From 2008 to 2010, he worked in the automotive industry for nearly two years, including an internship with FIAT Powertrain Technologies, and full-time working experience with the Delphi China Technical Center. From 2013 to 2016, he was a Postdoctoral Researcher with The University of Tokyo. He is currently a Lecturer with the School of Mechanical Engineering, Shanghai Jiao Tong University, Shanghai, China. His research interests include state estimation and control for electric vehicles.

Hiroshi Fujimoto (S'99–M'01–SM'12) received the Ph.D. degree from the Department of Electrical Engineering, The University of Tokyo, Chiba, Japan, in 2001.

In 2001, he joined the Department of Electrical Engineering, Nagaoka University of Technology, Niigata, Japan, as a Research Associate. From 2002 to 2003, he was a Visiting Scholar with the School of Mechanical Engineering, Purdue University, West Lafayette, IN, USA. In 2004, he joined the Department of Electrical and Computer Engineering, Yokohama National University, Yokohama, Japan, as a Lecturer and became an Associate Professor in 2005. Since 2010, he has been an Associate Professor with The University of Tokyo. His research interests include control engineering, motion control, nanoscale servo systems, electric vehicle control, and motor drives.

Dr. Fujimoto received Best Paper Awards from the IEEE TRANSACTIONS ON INDUSTRIAL ELECTRONICS in 2001 and 2013, the Isao Takahashi Power Electronics Award in 2010, and the Best Author Prize of the Society of Instrument and Control Engineers (SICE) in 2010. He is a Member of the SICE, the Robotics Society of Japan, and the Society of Automotive Engineers of Japan, and a Senior Member of the Institute of Electrical Engineers of Japan.

Shinji Hara (M'86–SM'04–F'06) received the B.S., M.S., and Ph.D. degrees in engineering from Tokyo Institute of Technology, Tokyo, Japan, in 1974, 1976, and 1981, respectively.

In 1984, he joined Tokyo Institute of Technology as an Associate Professor and then served as a Full Professor for ten years. Since 2002, he has been a Full Professor in the Department of Information Physics and Computing, The University of Tokyo, Tokyo. His current research interests include robust control, decentralized control for networked dynamical systems, global control, systems biology, and computational aspects of control system design.

Prof. Hara received the George S. Axelby Outstanding Paper Award from the IEEE Control Systems Society in 2006. He also received Best Paper Awards from SICE several times. He was the General Chair of CCA'04, the Program Cochair of the 17th IFAC World Congress, Seoul, South Korea, the President of SICE in 2009, the Vice-President of the IEEE CSS for membership activities in 2009–2010, has been an IFAC Council member since 2011, and an Associate Editor of several international journals including the IEEE TRANSACTIONS ON AUTOMATIC CONTROL and *Automatica*. He is a Fellow of IFAC and SICE.